The Large-Scale Morphology of IRAS Galaxies

Arif Babul[1], Glenn D. Starkman[1], & Michael A. Strauss[2]

[1] *Canadian Institute for Theoretical Astrophysics, Toronto, Canada.*

[2] *Institute for Advanced Study, Princeton, NJ.*

Introduction: At present, visual inspection is the only method for comparing the large-scale morphologies in the distribution of galaxies to those in model universes generated by N-body simulations. To remedy the situation, we have developed a set of three structure functions (S_1, S_2, S_3) that quantify the degree of large-scale prolateness, oblateness and sphericity/uniformity of a 3-D particle distribution (*c.f.* Babul & Starkman 1992, preprint) and have applied them to a volume-limited ($\leq 4000 \, \mathrm{km \, s^{-1}}$) sample of 699 IRAS galaxies with $f_{60} > 1.2 \, \mathrm{Jy}$ (Fisher 1992, Ph.D. Thesis, U.C. Berkeley).

To determine the structure functions, we randomly select 500 galaxies as origins of spherical windows of radius R_w, locate the centroid of the galaxies in the window (assuming all galaxies have equal mass) and then, compute the principal moments of inertia (I_1, I_2, I_3) about the centroid. Each S_i is a function of I_2/I_1 and I_3/I_1. S_1, S_2 and S_3 tend to unity for highly prolate, oblate and uniform distributions, respectively and tend to zero otherwise. The resulting 500 values of S_i at each scale R_w are used to construct a histogram.

IRAS Sample: In analyzing the IRAS sample, we restrict ourselves to windows with radius $1100 \, \mathrm{km \, s^{-1}} \leq R_w \leq 1700 \, \mathrm{km \, s^{-1}}$. Smaller windows contain too few galaxies while larger windows are rejected due to the scarcity of window origins for which the window lies entirely within the sample volume. A set of histograms for S_1, S_2 and S_3 in windows of radius $1300 \, \mathrm{km \, s^{-1}}$ is shown in panel 1 of Figure 1. The structures in the IRAS galaxy distribution do not appear to be highly prolate or oblate.

Model Distributions: We compare the IRAS results to analyses of eight galaxy distributions discussed by Weinberg & Cole (1991, preprint). The eight distributions correspond to particles identified as galaxies according to biased and unbiased schemes from simulations of an $\Omega = 1$ universe characterized by the initial 1-point probability distribution, $P(\delta)$, which is either Gaussian, or has a long tail of positive fluctuations (skew-positive), a long tail of negative density contrasts (skew-negative), or both negative and positive tails (broad). The non-Gaussian initial conditions were generated by a local transformation of the Gaussian field with power spectrum $P(k) \propto k^{-1}$. In order to ensure that S_i for the models are comparable to those for the IRAS galaxies, we analyze four subsets (spheres of radius $4000 \, \mathrm{km \, s^{-1}}$) of each of the simulation volumes, each containing 400—1000 galaxies. Placing the observer at the centre of the spheres, we transform the simulations from real space to redshift space. For each of the four volumes, we compute the S_i histograms at $R_w = 1100$, 1300, 1500, and $1700 \, \mathrm{km \, s^{-1}}$. For each S_i, the four histograms at a given R_w are then averaged to obtain the mean "model" histogram. Panels 2 and 3 of Figure 1 show the mean histograms for the unbiased Gaussian and the unbiased skew-positive models ($R_w = 1300 \, \mathrm{km \, s^{-1}}$).

Comparison: As a prelude to comparing the IRAS histograms to those for the models, we interpret the mean model histograms (for each S_i and at each R_w) as the underlying probability distributions and compute the likelihood (using the multinomial likelihood function) of obtaining the corresponding IRAS histogram. We also compute the likelihood for obtaining the histograms for each of the four spherical sub-volumes from the mean. The results for the two least unlikely models (unbiased skew-positive and unbiased Gaussian) are presented in Figure 2. The skew-positive model is preferred; its likelihood is the largest of any of the models and it is the only one for which the IRAS results are comparable to the likelihoods of individual volumes for all three S_i and at all R_w. The results of our likelihood analysis are evident in the histograms themselves. For example, in the Gaussian model, the histogram for S_1 ($R_w = 1300 \, \mathrm{km \, s^{-1}}$) has a tail extending to $S_1 = 0.3$ while both the skew-positive and IRAS histograms (compare panels in Figure 1) are narrower. The differences between the S_3 histograms are even more pronounced, with the Gaussian histogram being noticeably broader than either the IRAS or the skew-positive. The histograms for the latter two are similar. As an aside, we note that four out of five colleagues, when asked to visually compare unlabelled particle plots of the model galaxies to those for IRAS galaxies, also selected the unbiased skew-positive model as the most likely match.

Conclusions A preliminary comparison of the large-scale morphology of IRAS galaxies with those present in the eight simulated galaxy distribution suggests that the distribution of IRAS galaxies is most like the distribution of galaxies in an unbiased, evolved skew-positive model. This result suggests that either the initial conditions that gave rise to the IRAS galaxies are non-Gaussian or the nature of biasing associated with their formation gives such an impression.
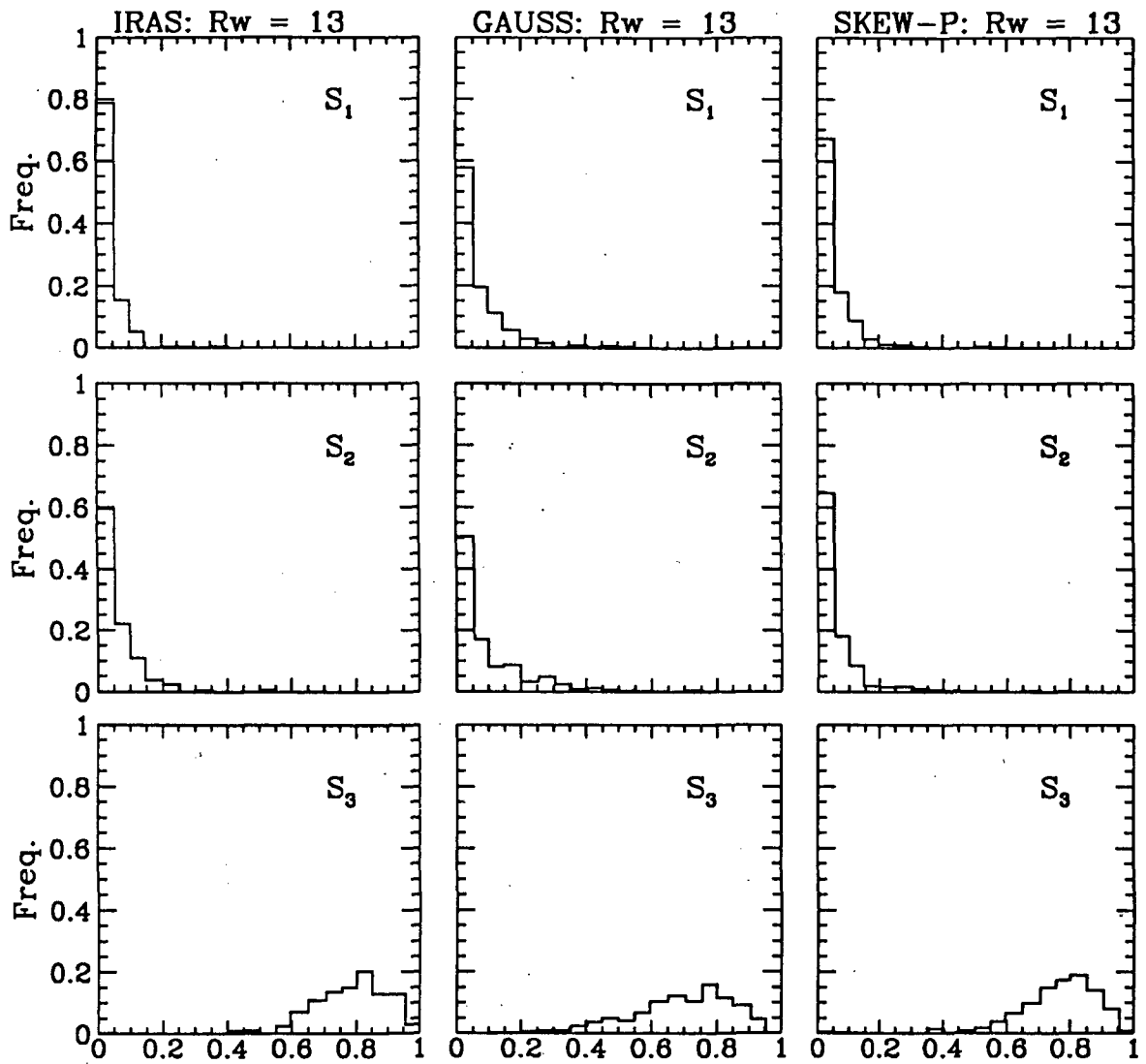
Fig. 1. Histograms for the normalized frequency distribution of S_i for IRAS galaxies (left column of panels) as well as for the galaxy distribution (unbiased) from simulations with Gaussian (middle column) and positively skewed (right column) initial 1-point probability distribution, $P(\delta)$.
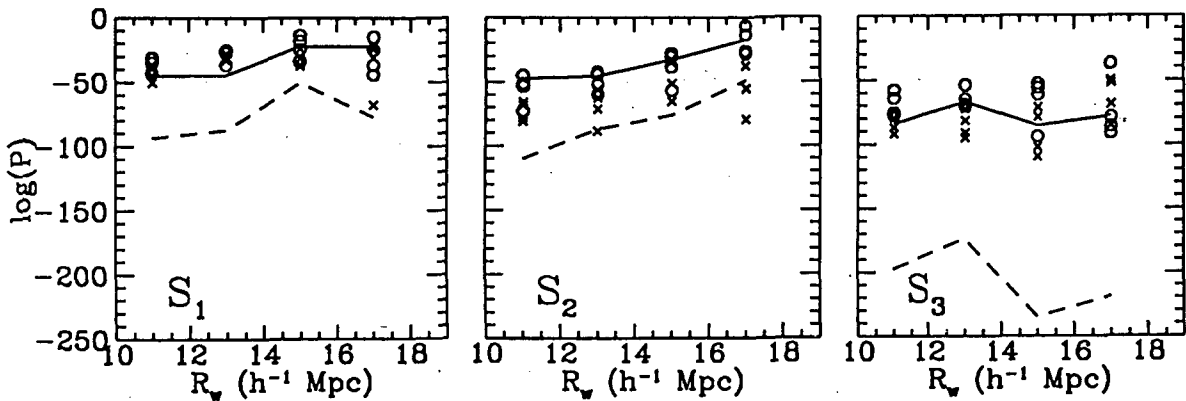

Fig. 2. The value of the likelihood function for obtaining the IRAS S_i histograms at $R_w = 1100, 1300, 1500,$ and $1700 \, \text{km s}^{-1}$ from the histograms for the skew-positive model (solid line) and for the Gaussian model (dashed line). The points show to the likelihood of obtaining the histograms for the four sub-volumes for each model from the mean histogram. The open circles correspond to the skew-positive model and should be compared to the solid line; the crosses correspond to the Gaussian simulation and should be compared to the dashed line.

59